BBAA VI International Colloquium on:
Bluff Bodies Aerodynamics & Applications
Milano, Italy, July, 20-24 2008

MODELING OF UNSTEADY TURBULENT FLOWS PAST ROUGHENED CIRCULAR CYLINDERS AND AIRFOILS

M. Mamou[*], M. Beyers[*], H. Dagdougui[§] and M. Hasnaoui[§]

[*]Institute for Aerospace Research
National Research Council, Ottawa, Ontario, K1A 0R6, Canada
e-mail: mahmoud.mamou@nrc-cnrc.gc.ca, martin.beyers@nrc-cnrc.gc.ca

[§]University Cadi Ayyad, Faculty of Sciences Semlalia, BP 2390 Marrakesh, Morocco
e-mail: hasnaoui@ucam.ac.ma

Keywords: Unsteady Turbulent Flows, Vortex Shedding, Roughness Effect & Stall

Abstract. *Under the dynamic stall project initiated recently at the Institute for Aerospace Research (IAR) of the National Research Council Canada (NRC), a thorough computational fluid dynamics (CFD) investigation of compressible flows past clean and rough cylinders and airfoils at low Mach numbers was undertaken. The objective was to assess the performance of a modified version of the FLOWer code in predicting steady/unsteady turbulent separated flows in the presence of surface roughness. Flow simulations were performed and analyzed using two-equation turbulence models, namely the Wilcox κ-ω and the modified Menter SST κ-ω with roughness modeling implementation. For unsteady flows past a rough cylinder, the drag coefficient and the Strouhal number agreed well with the experimental data. For steady state flows past airfoils, both turbulence models performed very well in predicting the maximum lift, when compared to experimental data for smooth and rough leading edges. For an airfoil with deployed flap, steady and unsteady flow solutions showed different flow patterns in the wake. The unsteady solution was characterized by vortex shedding, while the steady solution displayed a large flow recirculation region. The modified Menter SST κ-ω turbulence model performed much better than the Wilcox κ-ω model, as the former copes very well with strong adverse pressure gradients and massively separated flows. Studies of grid sensitivity and time-step size effects on the computed solutions were performed to assess the quality of the presented CFD data.*

1 INTRODUCTION

Surface contamination or roughness is known to have substantial effects on skin friction, heat transfer rate, and transition and separation locations. The effect of surface roughness on heat transfer rate in fully turbulent flows is of particular interest. For smooth wall flows, the laminar sub-layer represents the main impedance to heat transfer from the wall or towards it. For a rough wall, the roughness elements that protrude into the viscous sub-layer or extend beyond it enhance heat transfer rate through the increase in turbulence mixing. Many aerodynamic or hydrodynamic problems of engineering interest involve surface roughness, such as wind or gas turbine blades, atmospheric flows and heat exchangers. From the aerodynamics point of view, distributed roughness elements on wings or rotor blades resulting from ice accretion or insect contamination trigger earlier transition and also promote premature flow separation, causing notable drag increase and lift loss.

Accurate simulation of the roughness effects on fluid flow behavior and heat transfer relies on more advanced and often prohibitively intensive computational fluid dynamics (CFD) techniques. Large-eddy or direct-numerical simulations are the most promising techniques that can address accurately the physics of the flow past rough surfaces but they require large computational resources and are still restricted to simple geometric models at the academic level. To respond to engineering requirements in the design of any thermal or aerodynamic system, one has to resort to conventional CFD techniques, such as steady or unsteady Reynolds averaged Navier-Stokes (RANS or URANS) simulations. Surface roughness effects can be modeled through the adjustment of the turbulent boundary conditions near the wall surface, based on experimental observations. Wilcox [1] has covered this topic and demonstrated how the roughness effect could be implemented easily through the dissipation rate, ω, at the wall. Hellsten and Laine [2] showed that the Menter SST κ-ω turbulence model, in its original formulation, is not suitable for surface roughness modeling. They proposed and calibrated, through experiment, a new version of the Menter SST κ-ω turbulence model.

The literature is rich with experimental and theoretical investigations of low and high Reynolds number flows past smooth and rough circular cylinders or airfoils. As reported in Refs [3]-[4], thorough experimental investigations were presented for flows past cylinders, with either smooth or rough walls. For a given equivalent sand grain roughness height k_s, in the transcritical regime (according to Achenbach's definition [3]), the mean drag coefficient and Strouhal number were found to be almost constant and independent of the Reynolds number, while their asymptotic values, as well as the transition and separation locations were found to depend strongly on k_s. As most of the reported experimental data was uncorrected for wind tunnel blockage, it was difficult to make direct comparisons between the experimental and theoretical results in free air conditions. Nakamura and Tomonari (Ref. [5]) performed wind tunnel tests to investigate the effects of distributed surface roughness on flows past circular cylinders at high Reynolds numbers. The measured data were obtained for various geometric roughness heights k and corrected for wind tunnel blockage effects. However, the authors did not specify k_s for the various geometric roughness heights. Partial and fully rough cylinders were tested. Comparisons with the experimental data reported in Refs. [3]-[4] showed good agreement at approximately the same equivalent roughness height. More reliable wake blockage correction techniques have been developed recently for bluff-bodies in Ref. [6]. Improvement of the corrections to the measured data reported in Refs. [3]-[5] could facilitate the validation of CFD codes and enhance the quality of their predicted data. On the other hand, the flow simulations were conducted in free air conditions, which is still quite far from the true flow physics. Furthermore, the surface roughness, characterized by k_s is further hampering accurate CFD predictions owing to uncertainties resulting from incomplete experimental

information on the sand grain geometrical shape, surface distribution and height, separation and transition locations and other flow characteristics. In addition, it has been observed experimentally that the flow behavior depends strongly upon the free stream turbulence level (Refs [7]-[8]). It is well known that the flow behavior for the geometrically simple circular cylinder is highly complex, as it compasses many hydro-/aero-dynamics challenges. For accurate prediction of flows past smooth/rough cylinders, the flow unsteadiness due to the natural vortex shedding, and the moving transition and separation locations on the model surface, have to be taken into account.

A number of CFD investigations have been performed on flows past rough or smooth circular cylinders at relatively high Reynolds numbers using URANS or large eddy simulation (LES) approaches, see Refs. [9]-[13]. Although the comparisons of the predicted CFD results with the experimental data have been generally acceptable, noticeable discrepancies still exist in the drag coefficient, Strouhal number and other flow characteristics, such as transition and separation locations. Improvements to the experimental conditions, including comprehensive wall interference and roughness characterization, could improve the simulations. The modeling of turbulent unsteady flows with roughness effects is quite a challenge, as the turbulence models were developed and tuned for steady state flows. These are very demanding flows as it is impossible to address all the flow challenges using a single approach while modeling the true flow physics. Judging by the present trend, simulation of flows past cylinders will likely remain a challenge for many years to come. So far, according to the literature, there is understandably no consensus on what the acceptable discrepancies are to substantiate the accuracy of the CFD results.

The main purpose of the present paper was to demonstrate the applicability of the κ-ω turbulence models for steady and unsteady flows with wall roughness effect for cases where the wake flow is expected to be highly unsteady. The performance of the Wilcox κ-ω [1]-[2] turbulence models is explored in predicting the flow unsteadiness behavior past a fully rough circular cylinder at high Reynolds numbers, and the stall angle and maximum lift of the NACA 65_1-212 airfoil with rough leading edge, with/without a deployed flap. Results are presented in terms of lift and drag force coefficients, pressure coefficients, flow patterns, turbulence properties and Strouhal number. Comparisons with experimental data for both cylinder [3]-[5] and airfoil [14] were performed.

2 PROBLEM DESCRIPTION AND MATHEMATICAL MODEL

Fully turbulent flow simulations past a rough circular cylinder and for the NACA 65_1-212 airfoil with/without a deployed flap and clean or rough leading edges were performed using the Reynolds averaged Navier-Stokes equations in their unsteady form.

2.1 Governing turbulence equations and roughness modeling

The compressible viscous flow simulations solved the unsteady form of the Navier-Stokes equations with the low Reynolds two-equation κ-ω turbulence models. The Wilcox [1] κ-ω turbulence model, the original Menter SST κ-ω and the modified Menter SST κ-ω [2] turbulence models were utilized. It is well known that the Wilcox κ-ω turbulence model is sensitive to free stream turbulence, and thus unsuitable for free shear layer flows. The original Menter SST κ-ω turbulence model was proven to handle reasonably well separated flows or wall flows subject to significant adverse pressure gradients. In boundary layer flows over fully rough surfaces the boundary sub-layer does not exist, as the roughness induces local flow fluctuations, improving turbulence flow mixing. Near a rough wall, the Reynolds stresses become significant and cannot be neglected as in the case of a smooth wall flow. In

Wilcox's [1] roughness modeling, the value of ω is readjusted at the wall, which usually tends towards infinity for a smooth wall. For a rough wall, ω has a finite value and is prescribed as follows:

$$\omega_w = \frac{u_\tau^2}{\nu_w} S_R \tag{1}$$

where ω_w is the value at the wall, $u_\tau = \sqrt{\tau_w / \rho_w}$ is the friction velocity, and ν_w is the fluid kinematic viscosity. The roughness parameter S_R is defined as follows:

$$S_R = \begin{cases} \left(50 / k_s^+\right)^2 & \text{for} \quad k_s^+ < 25 \\ 100 / k_s^+ & \text{for} \quad k_s^+ \geq 25 \end{cases} \tag{2}$$

where $k_s^+ = u_\tau k_s / \nu_w$ and k_s are the dimensionless and dimensional equivalent sand grain roughness height. In the present paper, $k_s^+ = 5$ was prescribed over hydraulically smooth surface.

The Wilcox κ-ω turbulence model was found to perform well for flow simulation past a rough surface. However, the original Menter SST κ-ω turbulence model contains some deficiencies affecting the prediction of flow and turbulence properties over a rough surface. Hellsten and Laine [2] identified and proposed a new version of the Menter SST κ-ω turbulence model, called modified Menter SST κ-ω in this paper, which is suitable for flow simulation over a rough or smooth surface. Through comparison with experiment, the authors introduced a correction to the turbulent eddy viscosity by defining a new auxiliary function, F_3, as follows [2]:

$$\begin{aligned} \mu_T &= \frac{a_1 \rho \kappa}{\max(a_1 \omega; |\Omega| F_2 F_3)} \\ F_3 &= 1 - \tanh\left[\left(150\nu/(\omega d^2)\right)^4\right] \end{aligned} \tag{3}$$

where the function F_3 must be equal to zero near the wall and unity elsewhere. In the present paper, the actual value of the function F_3, given by the above expressions, and F_3=1 were considered for comparison.

3 NUMERICAL SOLUTIONS AND FLOW SOLVER

3.1 Grid generation and topology

The ICEM CFD package [15] was used to generate the structured multi-block grids around a circular cylinder and the airfoil with/without a deployed flap. The far field boundary was located at 50×L, where L=D (cylinder diameter) or L=C (airfoil chord length). As unsteady computations are CPU time intensive, parallel computations was carried out by using a large number of grid blocks (up to 22) of equal size. For the cylinder, combined O- and C-type grids were used. The O-grid was embedded within the C-grid as can be seen from Fig. (1a). This type of topology allowed the distribution of a large number of grid points around the cylinder with more clustering near the wall and along its expected wake region. There were 8 blocks around the cylinder, with a grid distribution of 33×141 each, and four blocks in the wake region totaling 241 grid points. The normal cylinder wall spacing was $\Delta r/D$=16×10^{-6}. For the airfoil configurations, as displayed in Fig. (1b), a C-type grid topology was used.

There were 510 grid points around the airfoil, 141 points from the wall to the far field and 141 points in the wake region. The normal spacing for this configuration was $\Delta y/C=(1.25\div3)\times10^{-6}$.

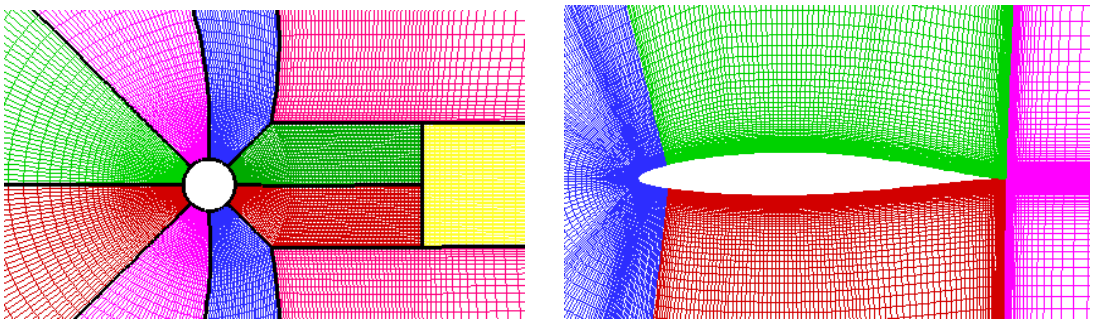

a) b)

Figure 1: Grid distribution: a) around a circular cylinder, b) around an airfoil.

3.2 Flow solver

The FLOWer code [16] was used for the flow simulations. This code solves the three-dimensional compressible RANS equations in their integral form for the low speed and high speed flow regimes. The turbulence is modeled by either algebraic or transport equation models. The numerical procedures are based on structured meshes, using either cell vertex or cell centered discretization schemes.

3.3 Boundary and flow conditions

In all flow configurations, uniform flow conditions were prescribed at the far field. No-slip smooth or rough wall conditions were applied on the models' surface. Two dummy cells were allowed at the block interfaces for flow properties exchange. For the cylinder configuration, the wall was entirely rough and characterized by an equivalent roughness height of $k_s/D=450\times10^{-5}$ [3]-[5]. Two Reynolds numbers were considered ($Re_D=10^6$ and 3×10^6). The far field turbulence level was set to 0.7% and 0.12% according to the Achenbach [3] and Nakamura and Tomonari [5] experiments, respectively. For the airfoil test case, carborundum grit was applied to the leading edge region, which extended to 8%C [14] from the leading edge. The sand roughness height was $k/C=45.83\times10^{-5}$. As the equivalent sand roughness height value for this particular configuration was unknown, $k_s=k$ was considered in the computations which, for the sparse roughness distribution on the airfoil leading edge, is considered a reasonable assumption. The Reynolds number was $Re_C=6\times10^6$.

3.4 Steady state flow solutions

For the steady state calculations, a cell-centered discretization was chosen. Jameson's central differencing scheme with explicit artificial dissipation was adopted to discretize the convective terms in the Navier-Stokes equations. A first-order upwind scheme (Roe) was used for solving the turbulence equations. The resulting discretized equations were solved using the explicit Runge-Kutta scheme for the Navier-Stokes equations and the DDADI-scheme for the turbulence equations. For more details about the flow solver and solution techniques, the reader is referred to Ref. [16]. Solution convergence was accelerated by the techniques of local time stepping and implicit residual smoothing. For enhancing the convergence, multi-grid algorithms were considered. A maximum CFL number of 10 was used, which was decreased to 5 when approaching stall conditions.

3.5 Unsteady state flow solutions

For time-accurate simulations, a fully implicit scheme was adopted. As implemented in the FLOWer code [16], the slightly modified Runge-Kutta algorithm, including all available acceleration techniques similar to a steady-state computation, was considered. This algorithm (called the dual time-stepping method) was characterized by inner or pseudo-time iterations within each physical time step. To compute unsteady flows past a cylinder or an airfoil configuration, a steady-state solution was first computed. This allowed the damping of all transient flow perturbations that could survive after using a uniform flow as initial condition. It was observed that acoustic waves were contaminating the flow region, and were taking a long time to dissipate. As the flow past a cylinder at high Reynolds number is fundamentally unsteady, the steady state computations could not converge within an acceptable residual magnitude drop, even though the drag coefficient was hovering around the mean value. The steady state solution was then fed into the solver as initial conditions, and the unsteady flow simulation was initiated. The computations were second-order accurate in time, which required two previous successive time levels to carry the computations to the new time level. However, when starting from a steady-state solution or from a solution obtained with different time step size, a first-order temporal scheme was used for the first time step. The dimensionless time step was chosen to be 0.0025-0.1, with inner iterations varying from 10 to 80 according to the prescribed convergence tolerance (5×10^{-5}, as a maximum residual) within each time step. In the FLOWer code, time was scaled according to $\tilde{t} = t\,(L/L_g)/\sqrt{RT_\infty}$, where L is the physical model length, L_g is the model length in the grid unit, R is the gas constant, T_∞ is the free stream temperature, and $\tilde{t}$ is the dimensional time.

4 RESULTS AND DISCUSSION

Two-dimensional numerical flow solutions are presented in terms of flow patterns and aerodynamic force coefficients. The configurations considered are a fully-rough circular cylinder in subsonic flow (M_∞=0.07) and the NACA 65_1-212 airfoil with/without a deployed flap and with smooth/rough leading edge, at a free stream Mach number of M_∞=0.14.

4.1 Flow past rough circular cylinder

To compare with the existing experimental data available in the literature, the predicted CFD results are presented for a high Reynolds number in the transcritical regime, where the boundary layer flow is dominated by turbulence. Starting with a steady-state solution, the flow evolved to the unsteady state where periodic flow oscillations were observed and vortex shedding occurred, as can be seen from the instantaneous vorticity magnitude contours in Fig. (2). The time histories of the drag and lift coefficients are displayed in Fig. (3) for $Re_D=10^6$. Two time series runs were executed. The first run was performed with a time step of $\Delta t = 0.1$, followed by the second one with $\Delta t = 0.01$ and then by a third run with $\Delta t = 0.0025$. The mean values of the drag and lift coefficients, the magnitudes of fluctuations, and the Strouhal number are given in Table 1 with comparison to experimental data reported in Ref. [5]. It was observed that the Wilcox κ-ω turbulence model underestimated the mean drag coefficient slightly and that the modified Menter SST κ-ω model overpredicted the mean value somewhat. This showed that the extent of the separation region is much larger for the case of the SST κ-ω model. As for the Strouhal number, it was the modified SST κ-ω model that gave the value closest to the experimental data. It is worth mentioning that the discrepancy of the original SST κ-ω predicted results relative to the experimental data was reasonable, albeit the largest. A snapshot of the flow streamlines obtained with the modified Menter SST κ-ω turbu-

lence model is displayed in Fig. (4). At that time instant, a fully formed vortex on the upper back side of the cylinder is observed.

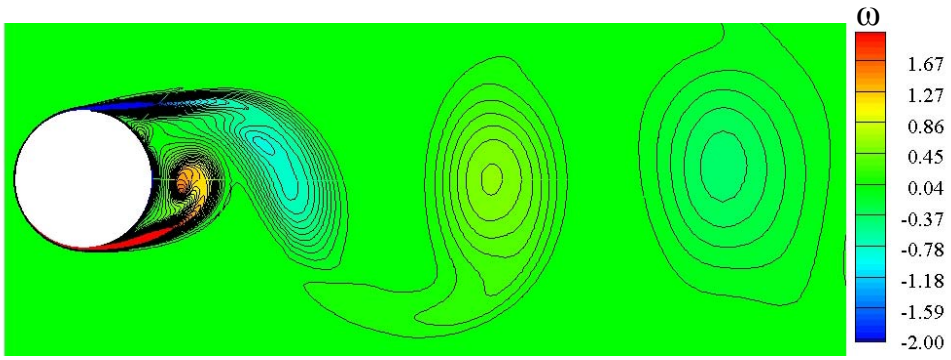

Figure 2: Snapshot of the flow vorticity contours around the rough circular cylinder and in the wake, using the modified Menter SST κ-ω turbulence model, for M_∞=0.07, k_s /D=450×10^{-5} and $Re_D = 10^6$.

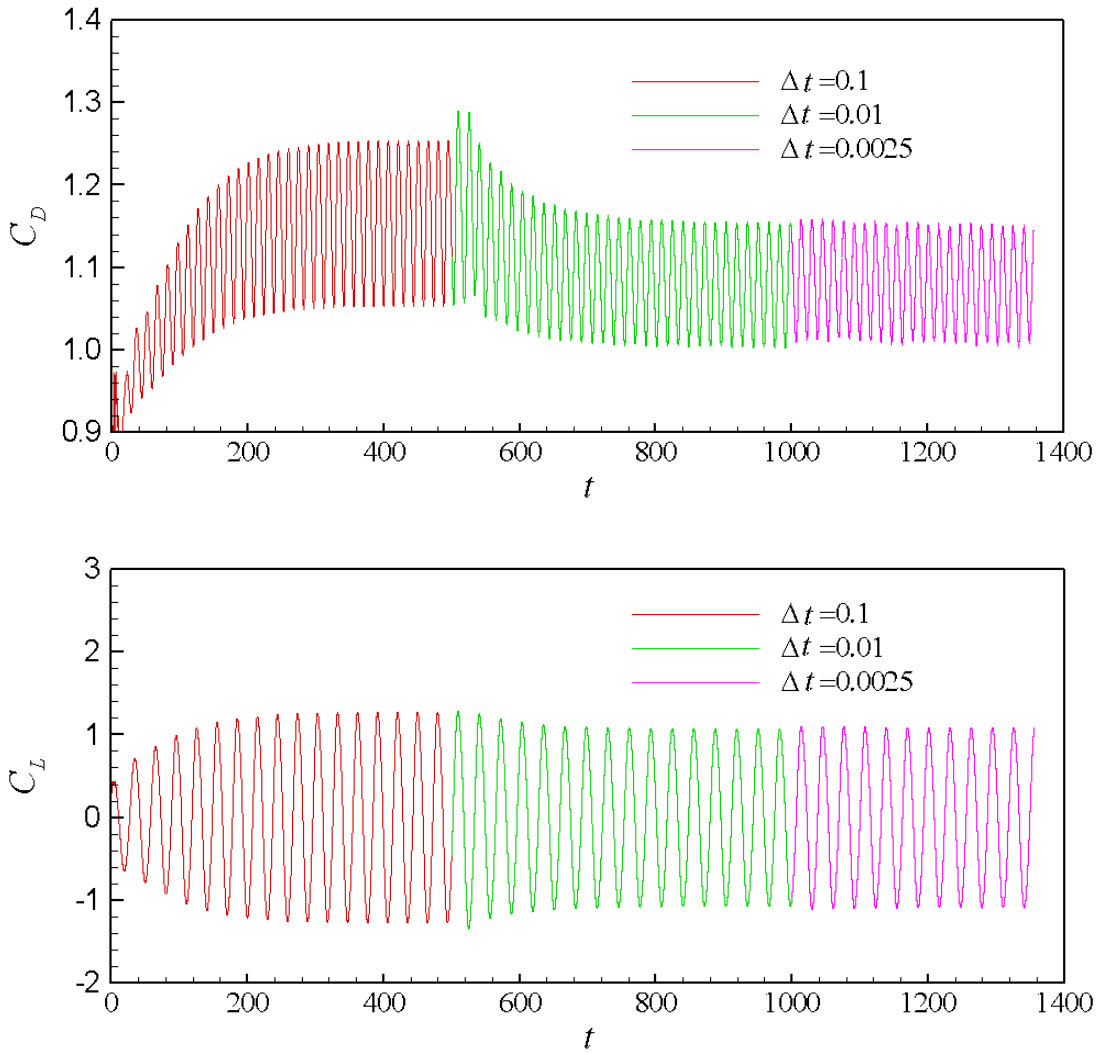

Figure 3: Time-history of the predicted drag (C_D) and lift (C_L) coefficients for a rough circular cylinder, obtained with the modified Menter SST κ-ω turbulence model, for M_∞=0.07, k_s /D=450×10^{-5} and $Re_D = 10^6$.

Grid sensitivity and time step size effect studies are reported in Tables 2 and 3, respectively. The numerical solutions were computed on the refined grid described in Section 3.1. A coarse grid solution was obtained by halving the number of grid points in both directions in each block. The wall normal spacing was roughly doubled. For the dense grid, the refined grid was obtained by doubling the number in both directions while keeping the same normal wall distance. According to the converged predicted results, it seems that the mean drag coefficient was approaching the experimental value. However, the Strouhal number experienced the opposite trend for the grid size effect. According to the mean drag coefficient, it can be seen that the difference in the results predicted by the refined and dense grid are close to each other. The refined grid was thus qualified to be adequate for accurate flow computations. For the time-step size effect, as displayed in Table 3 for $\Delta t = 0.1$, 0.01 and 0.0025, there was no significant change in the mean drag coefficient, the fluctuation amplitudes or the Strouhal number values. Thus $\Delta t = 0.01$ was adequate to capture the flow unsteadiness. The predicted CFD solutions with the three grids (coarse, refined and dense), as shown in Fig. (5), gave a reasonable distribution of $y^+ < 1.4$ for the turbulence models considered in the present study.

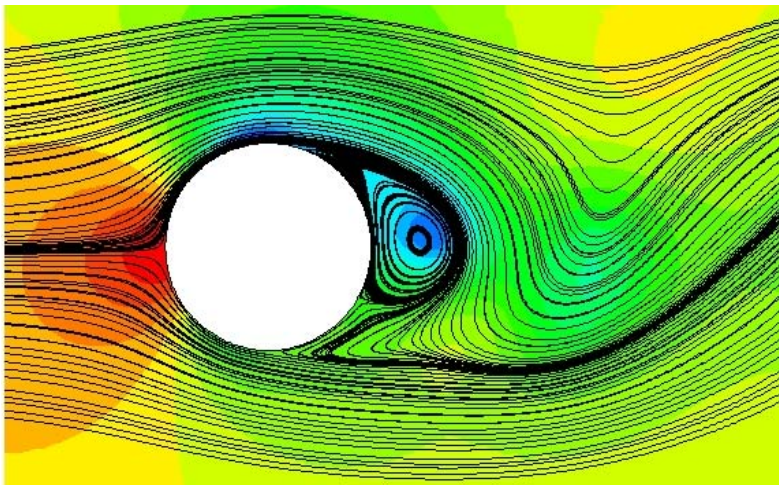

Figure 4: Snapshot of the flow streamlines and pressure distribution around the rough circular cylinder, obtained using the modified Menter SST κ-ω turbulence model, for M_∞=0.07, k_s/D=450×10^{-5} and $Re_D = 10^6$.

	Wilcox κ-ω	Original SST κ-ω, F_3=1	Modified SST κ-ω	Exp. [5]
C_{Dm}	0.9327	0.9866	1.0805	1.0420
rms (C_D)	0.0570	0.0611	0.0529	
rms (C_L)	0.7384	0.7660	0.7538	
St	0.2492	0.26378	0.2387	0.2110

Table 1: Comparison of the CFD predicted results with the experimental data for flows past a rough circular cylinder, obtained with the Wilcox κ-ω and original and modified Menter SST κ-ω turbulence models, for M_∞=0.07, k_s/D=450×10^{-5} and $Re_D = 10^6$.

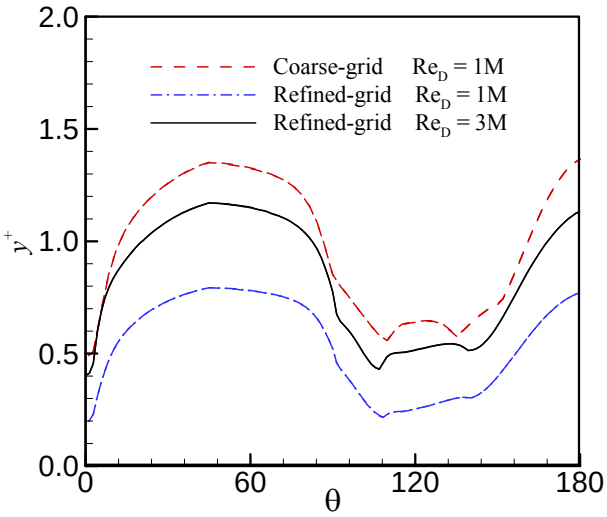

Figure 5: Time averaged y^+ profile around the rough circular cylinder for coarse and refined grids at $Re_D = 1\times10^6$ and 3×10^6, using the modified Menter SST κ-ω turbulence model.

	Coarse grid	Refined grid	Dense grid	Exp. [5]
C_{Dm}	1.2172	1.0805	1.0599	1.0420
rms (C_D)	0.0601	0.0529	0.0576	
rms (C_L)	1.0065	0.7538	0.7442	
St	0.2210	0.2387	0.2443	0.2110

Table 2: Grid sensitivity on the CFD predicted solutions for flows past a rough circular cylinder, obtained with the modified Menter κ-ω turbulence model, for M_∞=0.07, k_s/D=450×10^{-5} and $Re_D = 10^6$.

Δt	0.1	0.01	0.0025	Exp. [5]
C_{Dm}	1.1609	1.0805	1.0811	1.0420
rms (C_D)	0.0710	0.0529	0.0504	
rms (C_L)	0.9070	0.7538	0.7710	
St	0.2556	0.2387	0.2369	0.2110

Table 3: Effect of time step size on the CFD predicted results for flows past a rough circular cylinder, obtained with the modified Menter κ-ω turbulence model, for M_∞=0.07, k_s/D=450×10^{-5} and $Re_D = 10^6$.

To compare with the experimental data of Achenbach [3], a test case at Re_D= 3×10^6 was considered. For this particular value, the predicted results are displayed in Table 4 and compared to the corrected (C_{Dm}) and the uncorrected (C_{Dmu}) experimental data [4]. Both turbulence models predicted the drag fairly well. The time-averaged pressure coefficients are displayed in Fig. (6), where they are compared only to the available uncorrected experimental data for wind tunnel blockage. The trend is reasonably well predicted. The experimental separation location, obtained at zero mean skin friction, is within the range of the predicted results as displayed in Fig. (7). The CFD results showed that the separation location was moving periodically back and forth on the upper and lower surfaces of the cylinder. In terms of

turbulence model performance, the mean separation angle value, which is close to experiment, showed that the modified SST κ-ω turbulence model handled the unsteady flow separation well. As can be seen from Figs (4) and (6), the generated vortices created a small suction region on the back of the cylinder where the pressure dropped below the cylinder mean base pressure.

	Wilcox κ-ω	Modified SST κ-ω	Exp. [3]
C_{Dm}	0.9386	1.0555	C_{Dmu}=1.200, C_{Dm}=0.994
rms (C_D)	0.0577	0.0531	
rms (C_L)	0.6607	0.6786	
St	0.2488	0.2365	

Table 4: Comparison of the CFD predicted results with the experimental data for flows past a rough circular cylinder, obtained with the Wilcox κ-ω and modified Menter SST κ-ω turbulence models, for M_∞=0.07, k_s/D=450×10^{-5} and $Re_D = 3\times10^6$.

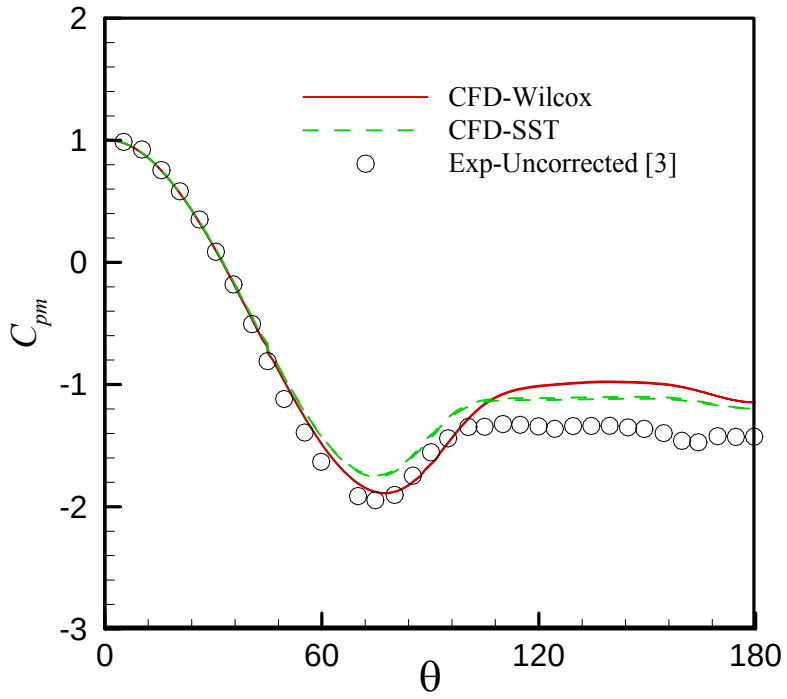

Figure 6: CFD time-averaged pressure coefficient profile on the rough circular cylinder at $\mathrm{Re}_D = 3\times10^6$, obtained with the Wilcox κ-ω and modified Menter SST κ-ω turbulence models, compared to the uncorrected measured data [3], for M_∞=0.07, k_s/D=450×10^{-5} and $Re_D = 3\times10^6$.

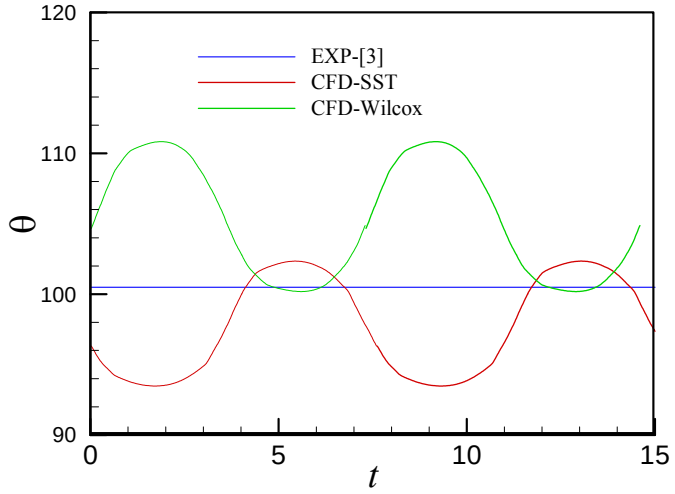

Figure 7: Separation angle over two periods of time, obtained with the Wilcox κ-ω and modified Menter SST κ-ω turbulence models, compared to the experimental data [3], for M_∞=0.07, k_s/D=450×10^{-5} and $Re_D = 3\times10^6$.

Using two-layer turbulence modeling, with a κ-ω turbulence model near the cylinder region and a κ-ε turbulence model far away from the cylinder, Pontaza et al. [10] performed flow simulations around a smooth and a rough cylinder for $k_s / D = 250\times10^{-5}$ and $Re_D = 10^6$. The authors predicted periodic oscillatory flows. The computed mean drag for both cases was overestimated when compared to the experimental data reported by Achenbach [3]. As noted in Ref. [12], it was not evident that LES simulation had improved the CFD predictions appreciably. The CFD results were fairly well predicted by comparing with the experimental results. However, the causes of existing discrepancies were not identified. Even grid refinement did not help to improve the accuracy of the CFD results. As in the present investigation, the grid refinement resulted in a slight divergence of the predicted Strouhal number from the experimental data. Investigation of the use of turbulence models for flows simulation past a smooth cylinder in crossflow was discussed in Ref. [17]. The authors used the κ-ω turbulence models and noticed that significant discrepancies remained between the predicted results and the experimental data. To improve the comparisons, the authors suggested improving the eddy-viscosity modeling. The experimental data reported in the past need to be reconsidered, using the appropriate wind tunnel blockage corrections, such as that proposed in Ref. [6]. This may reduce the discrepancies between CFD predictions and measured data.

4.2 Flow past airfoil near stall

The numerical solutions were based on RANS and URANS calculations. Comparisons with experimental airfoil data [14] were performed and results were presented in terms of the force coefficients, pressure coefficients and flow patterns for a simple NACA 65$_1$-212 airfoil and for the airfoil with a split flap deployed at 60^o with respect to the chord line. The viscous grid distribution is displayed in Fig. (1b) for the simple airfoil, and in Fig. (8), for the airfoil with deployed flap. A maximum value of y^+ of about 1.2 or less was obtained at the first grid point from the wall. At the airfoil maximum lift, y^+ was increased to 1.4 near the suction peak. The dimensionless time step was chosen to be 0.001–0.01, with inner iterations varying from 10 to 80, according to the prescribed convergence tolerance within each time step (i.e. 5×10^{-5}).

Figure (9) displays the convergence history of the airfoil lift coefficient and the density residual variation as a function of the iteration number. The flow solution was obtained for a rough leading edge at an angle of attack of 11°, where trailing edge stall occurred. The CFL number used for this simulation was 5. As expected, when approaching stall, the convergence becomes difficult and the residual drop decreases. For this particular angle of attack, the residual dropped by about 4 orders of magnitude to reach a constant lift coefficient, as can be seen from Fig. (9). Owing to flow separation, which is difficult to predict with turbulence modeling, the residual was seen to oscillate and hover around a constant value. The trailing edge separation region is quite visible in Figure (10), which displays the Mach number distribution and streamlines around the airfoil at the same angle of attack (α=11°).

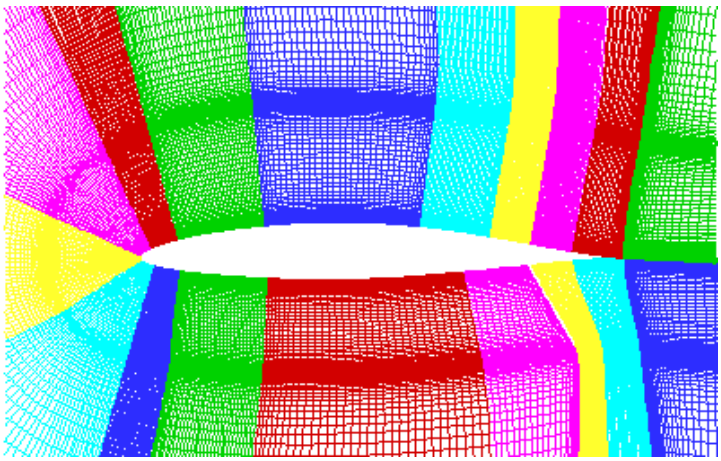

Figure 8: Grid distribution around the airfoil with deployed flap.

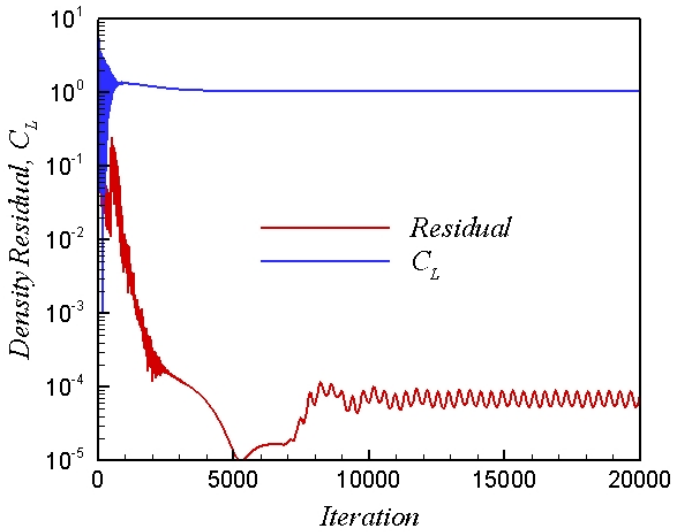

Figure 9: Lift coefficient and density residual history for the airfoil with rough leading edge, for α=11°, M_∞=0.14, k_s/D=45.83×10^{-5} and Re_C =6×10^6 (steady state solution).

Figure (11) shows the airfoil lift coefficient variation with angle of attack for clean and rough leading edges, demonstrating that trailing edge stall occurred at lower angles of attack for the rough case, reducing the maximum lift coefficient. Overall good agreement was ob-

served between the simulations and the experimental data [14] for smooth or rough leading edges, for both turbulence models considered in the present study. Comparing the predictions obtained using the two turbulence models, it appears that the modified Menter SST κ-ω turbulence model predictions for the lift coefficient were slightly below the Wilcox ones (Figure 11). However, the results from both models agreed well with the experimental data. A similar trend was reported in Ref. [2] for another type of airfoil. It should be noted that exact agreement was not expected as 3D flow effects were unavoidable in the experiment near stall conditions. It is clear that the original version of the Menter SST κ-ω turbulence model (F_3=1) over-estimated the maximum lift coefficient and the corresponding stall angle. Thus, for roughness modeling, it is recommended that the modified version of the SST κ-ω turbulence model developed in Ref. [2] be considered.

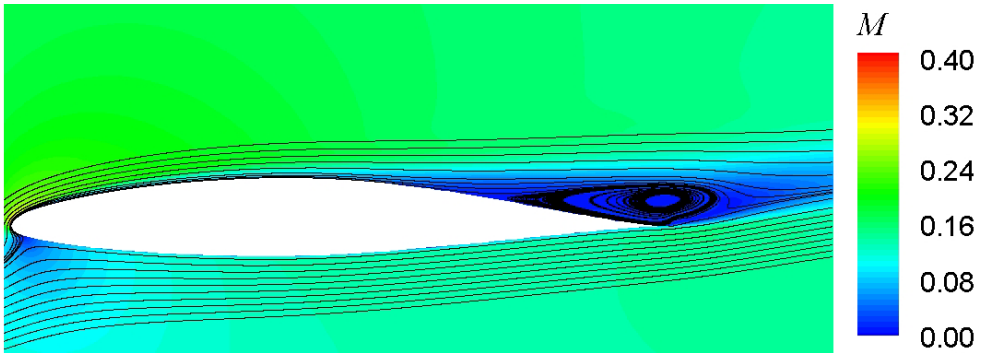

Figure 10: Mach number distribution around the airfoil with rough leading edge, α=11°, for M_∞=0.14, k_s/D=45.83×10^{-5} and $Re_C = 6\times10^6$ (steady state solution).

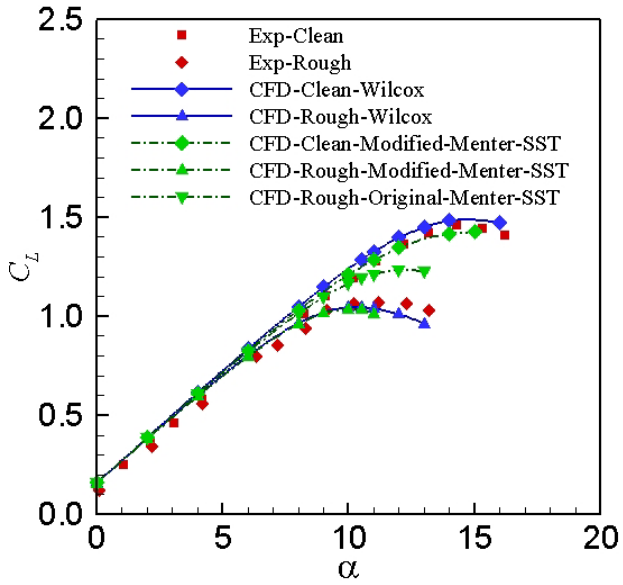

Figure 11: Lift coefficient versus angle of attack for the airfoil with clean and rough leading edges, for M_∞=0.14, k_s/D=45.83×10^{-5} and $\mathrm{Re}_C = 6\times10^6$ (steady state solution).

The Mach number distribution and streamlines for the airfoil with a deployed flap are presented in Fig. (12). The lift coefficient versus angle of attack is illustrated in Fig. (13), using

the modified Menter SST κ-ω turbulence model. Owing to the presence of the flap, the flow was massively separated near the trailing edge region (Fig. 12), with a large recirculation zone. For this flow configuration, the flow solver convergence was difficult, as the flow was expected to be highly unsteady. The maximum lift was underestimated, which could have been caused by early flow separation on the upper surface of the airfoil trailing edge triggered by the huge recirculation zone, where turbulence modeling would be meaningless. The unsteady computations, illustrated by the Mach number contours in Fig. (14), show that vortices are periodically shed from the airfoil and flap trailing edge, leading to a complex flow structure behind the airfoil. With second-order accuracy in time and space, the vortices generated may not be well resolved owing to numerical dissipation, which smears the vortex, lowering its intensity and enlarging its size. This obviously had an adverse effect on the stall behavior near the airfoil trailing edge. The unsteady computations showed flow patterns in the airfoil wake different from their steady state counterparts. While in the steady case the wake was characterized by a large recirculation zone, in the unsteady case, a series of shed vortices was observed.

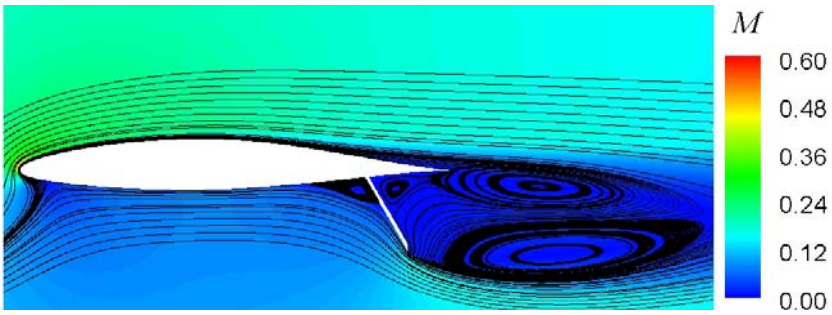

Figure 12: Mach number distribution and streamlines around clean leading edge airfoil with deployed flap, at α=9.5°, obtained with the modified Menter SST κ-ω turbulence model, for M_∞=0.14, k_s/D=45.83×10^{-5} and $\mathrm{Re}_C = 6\times10^6$ (steady state solution).

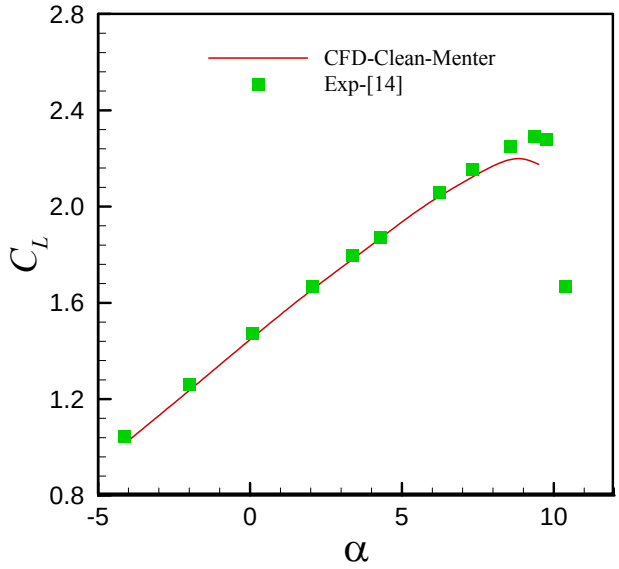

Figure 13: Lift coefficient versus the angle of attack for clean leading edge airfoil with deployed flap, obtained with the modified Menter SST κ-ω turbulence model, for M_∞=0.14, k_s/D=45.83×10^{-5} and $Re_C = 6\times10^6$ (steady solution).

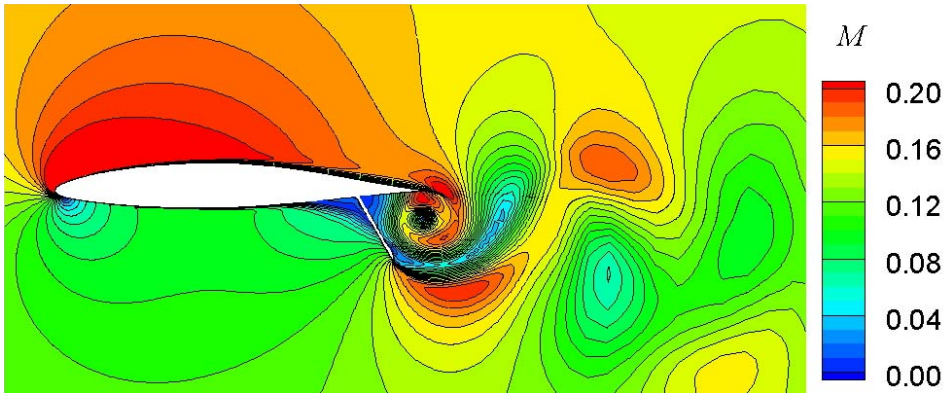

Figure 14: Snapshot of the unsteady flow past the clean leading edge airfoil with deployed flap, at α=4°, obtained with the modified Menter SST κ-ω turbulence model, for M_∞=0.14, k_s/D=45.83×10^{-5} and $Re_C = 6\times10^6$.

5 CONCLUSIONS

- The Wilcox k-ω and the modified Menter SST k-ω turbulence models, both modified to include physical roughness effects, were validated against experimental data. The computed drag and the Strouhal number for a rough circular cylinder showed reasonably good agreement with the experimental data. Satisfactory agreement with experiment was obtained for an airfoil, showing the premature stall and loss of maximum lift coefficient induced by leading-edge roughness.
- The flow past a rough circular cylinder is a great challenge as it involves phenomena including steady/unsteady laminar flows, transitional flows, turbulent flows, massively separated flows, vortex shedding, and moving transition and separation locations. Using CFD simulation through turbulence and roughness modeling for such complex flows may lead to inaccurate flow physics predictions.
- For the cases of the clean or rough airfoil, as well as for the rough cylinder, good results can be obtained from an unsteady RANS flow solver incorporating a suitable roughness module.
- From an engineering point of view and according to the present CFD predicted results, the Navier-Stokes equations with the Wilcox κ-ω and the modified Menter SST κ-ω turbulence models can give fairly good results for bluff body flow simulations and for airfoils stall prediction.

ACKNOWLEDGEMENTS

The authors would like to thanks Dr. Jochen Raddatz and Dr. Thorsten Schwarz from DLR-Institut für Aerodynamik und Strömungstechnik for their support in running and developing the DLR FLOWer code for roughness modeling. This project is supported internally by the Aerodynamics Laboratory and the Flight Research Laboratory within IAR/NRC.

REFERENCES

[1] D.C. Wilcox. *Turbulence Modeling for CFD*, DCW Industries Inc., 2nd Edition, 1998.

[2] A. Hellsten and S. Laine. Extension of the k-ω-SST Turbulence Model for Flows over Rough Surfaces, AIAA-97-3577, 252-260, 1997.

[3] E. Achenbach. Influence of Surface Roughness on the Cross-Flow around a Circular Cylinder, *Journal of Fluid Mechanics*, **46**, 321-335, 1971.

[4] E. Achenbach and E. Heinecke. On Vortex Shedding from Smooth and Rough Cylinders in the Range of Reynolds Numbers 6×10^3 to 5×10^6, *Journal of Fluid Mechanics*, 109, 239-251, 1981.

[5] N.Y. Nakamura and Y. Tomonari. The Effects of Surface Roughness on the Flow Past Circular Cylinder at High Reynolds Numbers, *Journal of Fluid Mechanics*, **123**, 363-378, 1982.

[6] K.R. Cooper, E. Mercker and J. Wiedemann. Improved Blockage Corrections for Bluff Bodies in Closed and Open Wind Tunnels, Proceedings of the 10th International Conference on Wind Engineering, Copenhagen, Denmark, June 21-24, 1999.

[7] B.A. Jubran, M.N. Hamdan and B.O. Al Bedoor. Roughness and Turbulence Intensity Effects on the Induced Flow Oscillation of a single Cylinder, *Applied Scientific Research*, 49, 101-115, 1992.

[8] S.J. Zan and K. Matsuda. Steady and Unsteady Loading on a Roughened Circular Cylinder at Reynolds Numbers up to 900000, *Journal of Wind Engineering and Industrial Aerodynamics*, **90**, 567-581, 2002.

[9] D. Lakehal. Computation of Turbulent Shear Flows over Rough-Walled Circular Cylinders, *Journal of Wind Engineering and Industrial Aerodynamics*, 80, 47-68, 1999.

[10] J.P. Pontaza, H.C. Chen, and C.R. Chen. Numerical Simulations of Riser Vortex-Induced Vibrations, Proceedings, SNAME Maritime Technology Conference & Expo and Ship Production Symposium, Houston, Texas, October 19-21, 2005.

[11] J.P. Pontaza and H.C. Chen. Three-Dimensional Numerical Simulations of Circular Cylinders Undergoing Two Degree-of-Freedom Vortex-Induced Vibrations, Transactions of the ASME, 129, 158-164, 2007.

[12] M. Breuer. *Large Eddy Simulation of High Reynolds Number Circular Cylinder Flow*, Chapter in the book on Industrial and Environmental Applications of Direct and Large-Eddy Simulation, **529**, 176-189, 1999.

[13] P. Catalano, M. Wang, G. Iaccarino and P. Moin. Numerical Simulation of the Flow Around A circular Cylinder at High Reynolds Numbers, *International Journal of Heat and Fluid Flow*, **24**, 463-469, 2003.

[14] H. Abbott, A.E. von Doenhoff and L.S. Stivers. Summary of Airfoil Data, NACA Report, No. 824, 1945.

[15] ICEM CFD Package, http://www.ansys.com/products/icemcfd.asp.

[16] FLOWer Installation and User Handbook, Institute of Aerodynamics and Flow Technology of the German Aerospace Center (DLR), Doc. Nr. MEGAFLOW-1001.

[17] M.E. Young and A. Ooi. Turbulence Models and Boundary Conditions for Bluff Body Flow, 15th Autralasian Fluid Mechanics Conference, Sydney, Australia, December 13-17, 2004.